

Molecular Topology Applied to the Discovery of 1-Benzyl-2-(3-fluorophenyl)-4-hydroxy-3-(3-phenylpropanoyl)-2H-pyrrole-5-one as a Non-Ligand-Binding-Pocket Antiandrogen

Laura Caboni,^{*,†,||} Maria Gálvez-Llompart,^{*,‡} Jorge Gálvez,[‡] Fernando Blanco,[†] Jaime Rubio-Martínez,[§] Darren Fayne,[†] and David G. Lloyd^{†,‡}

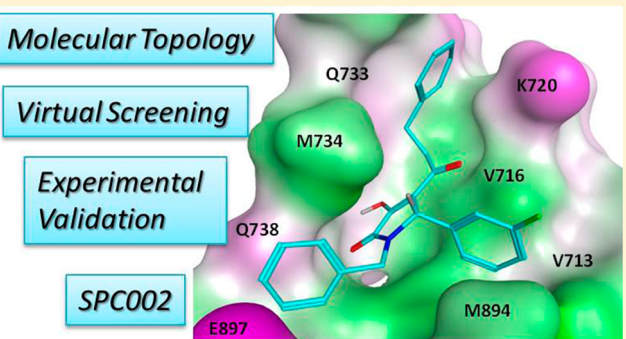
[†]Molecular Design Group, School of Biochemistry and Immunology, Trinity Biomedical Sciences Institute, Trinity College Dublin, Dublin 2, Ireland

[‡]Drug Design & Molecular Connectivity Research Unit, Department of Physical Chemistry, Faculty of Pharmacy, University of Valencia, Burjassot, Valencia, Spain

[§]Department of Physical Chemistry and Instituto de Química Teórica y Computacional (IQTQUB), University of Barcelona (UB), Barcelona, Spain

Supporting Information

ABSTRACT: We report the discovery of 1-benzyl-2-(3-fluorophenyl)-4-hydroxy-3-(3-phenylpropanoyl)-2H-pyrrole-5-one as a novel non-ligand binding pocket (non-LBP) antagonist of the androgen receptor (AR) through the application of molecular topology techniques. This compound, validated through time-resolved fluorescence resonance energy transfer and fluorescence polarization biological assays, provides the basis for lead optimization and structure–activity relationship analysis of a new series of non-LBP AR antagonists. Induced-fit docking and molecular dynamics studies have been performed to establish a consistent hypothesis for the interaction of the new active molecule on the AR surface.



INTRODUCTION

Traditional nuclear receptor (NR) drug discovery has been focused at the core of the C-terminal 12- α -helical ligand binding domain (LBD), the ligand binding pocket (LBP), where natural ligands bind and drive conformational changes that are necessary for NR transcriptional activity.¹ In response to ligand binding to the LBP, the hydrophobic activation function 2 (AF-2), involving helices 3, 4, 5, and 12, is generated to allow the recruitment of coactivator proteins that ultimately have consequences in NR functional activity (Figure 1). Additional allosteric regulatory interfaces, such as binding function-3 (BF-3), have been described for the androgen receptor (AR).²

Alternative AR targeting through its regulatory interfaces has gained a great deal of attention over the past decade.^{4–9} The need for such approaches arises from the limitations of currently marketed LBP-acting antiandrogens, especially in castrate-resistant prostate cancer (CRPC), wherein through receptor mutation in the LBP, hitherto antiandrogenic moieties are subsequently accommodated as androgenic species. Alternative targeting directed at non-LBP interfaces is intended to overcome some of these limitations. Specifically, protein–protein interactions at the NR AF-2 interface are mediated by short-sequence signature motifs (NR boxes) composed of five

amino acids, usually of the type LxxLL. AR has been shown to preferentially accommodate bulkier side-chain motifs, such as the FxxLF motif. These motifs can be effectively mimicked by peptides and small molecules to repress AR transcriptional activity.^{9–11} Different scaffolds targeting non-LBP regulatory surfaces have been identified by means of different techniques, such as high-throughput screening, virtual screening, structure-based drug design, and X-ray crystallography.^{10–15} The small molecules identified to date lack potency,¹⁶ hence the constant need for novel scaffolds to support enhanced ligand-based drug discovery efforts. Here we report the discovery of a novel scaffold, 1-benzyl-2-(3-fluorophenyl)-4-hydroxy-3-(3-phenylpropanoyl)-2H-pyrrole-5-one, through the application of molecular topology (MT) techniques.

Quantitative structure–activity relationship (QSAR) studies are widely used in drug design and discovery; this methodology can contribute to a reduction in the number of costly failures of drug candidates in clinical trials by presynthesis filtering of virtual combinatorial libraries. Through such approaches, druglike or leadlike compounds with predicted adverse

Received: June 1, 2014

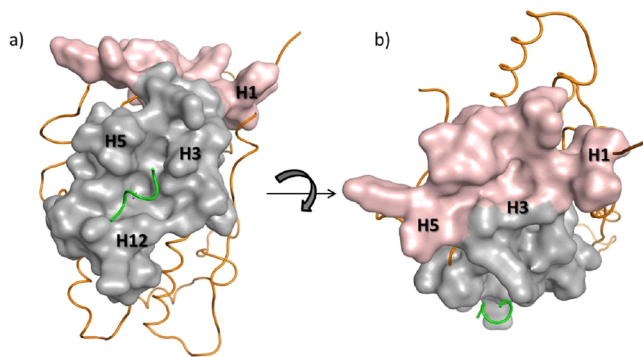


Figure 1. Activation function 2 (AF-2) and binding function 3 (BF-3) regulatory interfaces of the androgen receptor (AR). (a) Structure of AR LBD AF-2 (surface color: gray) with bound coactivator (green ribbon) and adjacent surface BF-3 (surface color: pink). (b) BF-3 top view after rotation of the AR LBD on the x axis. Helices H1, H3, H5, and H12 are highlighted in both structures. PDB ID: 1T7R. Images were generated with Molecular Operating Environment (MOE 2011.10).³

toxicity^{17–19} or poor pharmacokinetic properties²⁰ can be identified early in the pipeline and removed from consideration.

In previous studies, we successfully applied topological descriptors^{21–25} as variables in QSAR approaches. MT is the topological description of molecular structures in terms of connectivity, and it is expressed in terms of numerical descriptors that are invariant under deformation of the structure. Topological indices (TIs) are “numbers that characterize a specific aspect of a molecule”.²² One of the advantages of MT is the fast and accurate prediction of many physicochemical^{26–30} and biological^{31–58} properties. Furthermore, topological descriptors have been applied to predict potential side effects of drug candidates,^{59,60} and several patents have been derived from the application of MT as a computer-aided drug design (CADD) approach.^{61–65}

The present work is the first to utilize connectivity data of small molecules characterized in the literature as non-LBP antiandrogens to identify a novel chemical scaffold with the desired biological activity that is amenable to optimization for its potential application in treatment of CRPC and for future ligand-based approaches directed at the AR regulatory surfaces. In so doing, this work confirms the feasibility of molecular topology applications as a parallel drug discovery strategy to provide novel molecular scaffolds based on existing ligand knowledge.

■ MOLECULAR TOPOLOGY PROTOCOL

Our MT/virtual screening protocol for identifying novel AR antagonists included the following steps (Figure 2):

- Selection of data sets from the literature or experimental analysis. These data sets include all of the compounds used to build the models.
- Calculation of topological descriptors using Dragon software.⁶⁶
- Splitting of the data into two groups: an active set and an inactive set.
- Application of linear discriminant analysis (LDA) to the training set.
- Experimental validation of the LDA models.
- Application of the topological models to screen a subset of newly synthesized AR-targeting compounds.

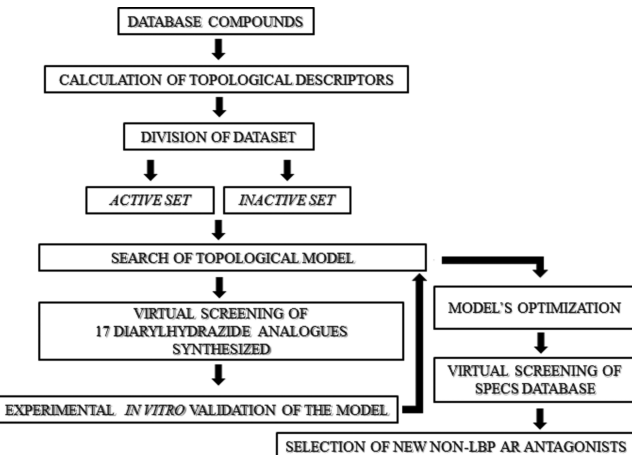


Figure 2. Scheme of the application of molecular topology and virtual screening in finding novel non-LBP AR antagonists.

- Model optimization.
- Virtual screening of the SPECS commercial ligand database.⁶⁷

Selection of Data Set. To assemble the mathematical models, we included a total of 52 compounds [MDG001–MDG052] belonging to three related scaffolds of the diarylhydrazide family (Figure 3), which was recently identified

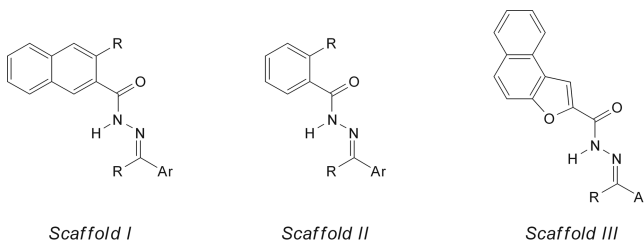


Figure 3. Molecular scaffolds previously studied by our group as non-LBP AR antagonists:¹¹ the (I) naphthyl, (II) phenyl, and (III) naphtho[2,1-*b*]furan-2-yl series.

by our group as a non-LBP AR antagonist scaffold. Nine of these compounds were found to be active in disrupting the AR–coactivator interaction (Figure 4).¹¹ Six of them (MDG001, MDG007, MDG008, MDG009, MDG010, and MDG023) belong to the naphthyl scaffold (scaffold I), and three (MDG038, MDG043, and MDG048) belong to the naphtho[2,1-*b*]furan-2-yl scaffold (scaffold III) (see the Supporting Information). All of the compounds belonging to the phenyl scaffold (scaffold II) were inactive.

As SAR was additionally explored for the MDG series of diarylhydrazides, we included 17 synthesized analogues to validate the mathematical models. These compounds are shown in Table 1. Additionally, in order to refine the topological models, we included all of the other compounds that were reported in the literature as non-LBP AR antagonists (Figure 5): (a) mixed AF-2/BF-3 compounds reported by Estebanez-Perpina et al.² [ESTB001–ESTB009]; (b) AR-selective peptidomimetic pyrimidines reported by Gunther et al.¹⁰ [GNT001–GNT014]; (c) AF-2-selective small molecules reported by Axerio-Cilie et al.¹² [AXE001–AXE006]; and (d) BF-3-selective small molecules reported by Lack et al.¹³ [LCK001–LCK009]. In total, 90 compounds presenting 15

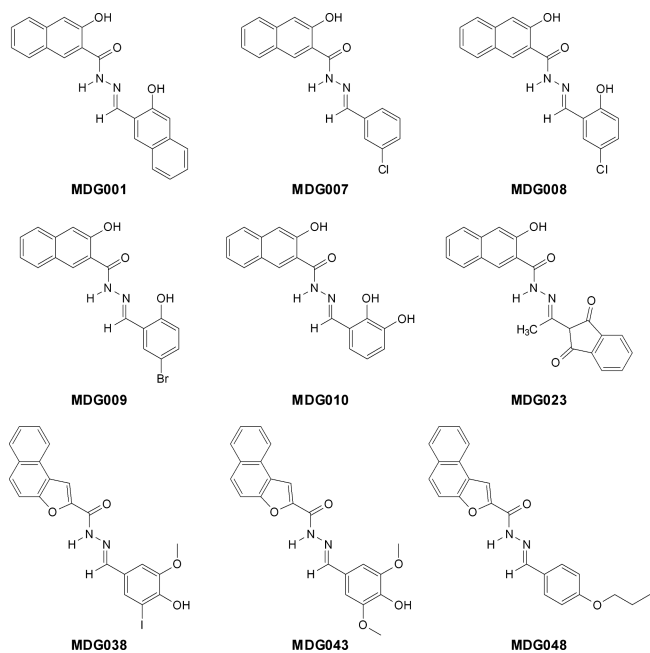


Figure 4. Active compounds identified in the MDG series. Six of them (MDG001, MDG007, MDG008, MDG009, MDG010, and MDG023) belong to the naphthyl scaffold (scaffold I), and three (MDG038, MDG043, and MDG048) belong to the naphtho[2,1-*b*]furan-2-yl scaffold (scaffold III).

Table 1. Series of 17 Novel Diarylhydrazide Analogues Included in the Topological Models

compound	R ₁	R ₂	R ₃	R ₄	R ₅	R ₆
MDG053	OH	H	H	H	Cl	NO ₂
MDG054	OH	H	OH	H	H	H
MDG055	OH	H	OH	H	H	CH ₃
MDG056	OH	H	OH	H	H	C(CH ₃) ₃
MDG057	OH	H	OH	H	H	OH
MDG058	OH	H	OH	H	H	OCH ₃
MDG059	OH	H	OH	H	H	I
MDG060	OH	H	OH	H	H	NO ₂
MDG061	OH	H	OH	CH ₃	H	H
MDG062	OH	H	OH	OCH ₃	H	H
MDG063	OH	H	OH	Cl	H	H
MDG064	OH	H	OCH ₃	H	H	H
MDG065	OH	H	OCH ₃	H	H	Br
MDG066	OH	CH ₃	OH	H	H	Cl
MDG067	OH	H	OH	H	H	H
MDG068	H	H	OH	H	H	Cl
MDG069	OH	H	OH	OCH ₃	H	Cl

different scaffolds were included in the model. Of these, just over half ($n = 47$) had an experimentally determined IC_{50} between ~ 1 and $50 \mu\text{M}$ in inhibiting the AR LBD as measured by direct binding assays or a functional reduction in AR transcriptional activity.

EXPERIMENTAL SECTION

Mathematical Modeling Equations. The MT protocol to predict novel scaffolds as non-LBP AR antagonists included four equations. Each of them presents a different training set composed of molecules that are topologically similar to the test set, as explained below:

(a) Equation 1 was a general model to identify non-LBP AR antagonists, which included 89 compounds. Of these, 47 were known non-LBP AR antagonists^{2,10,12,13} and 42 were “inactive” compounds (i.e., compounds for which no known AR activity is described in the literature) belonging to different classes such as anti-inflammatory, antiarrhythmic, anticonvulsant, anxiolytic, antiglaucoma, analgesic, and antimarial.

(b) Equation 2 was designed specifically to identify non-LBP AR antagonists by using our groups’ self-generated experimental data. This model included 52 compounds, of which nine were active and the remaining 43 did not display non-LBP AR antagonistic activity in our experimental assays.

(c) Equation 3 was based on all of the experimental data sets obtained while screening for non-LBP antiandrogens in published studies by our group, including the active compounds from a newly synthesized series of diarylhydrazides (Table 1). Therefore, the active set was composed of 15 compounds and the inactive set was composed of 54 compounds.

(d) Equation 4 was based solely on the experimental results for a new series of 17 diarylhydrazide analogues belonging to MDG scaffold 1 [MDG053–MDG069] (Table 1) that were synthesized by our group on the basis of pure chemical SAR criteria and were evaluated experimentally. Six compounds were found to be active as AR antagonists while 11 compounds were inactive.

The compounds used to build our models are shown in Tables S1–S5 in the Supporting Information. All of the data sets are characterized by large structural diversity.

Molecular Descriptors. The 2D structure of each compound was built using ChemBioDraw Ultra version 12.0¹⁵ (CambridgeSoft Corporation, Cambridge, MA). Each compound was characterized by a set of TIs, such as topological descriptors,⁶⁸ edge adjacency indices,⁶⁸ topological charge indices,⁶⁹ 2D autocorrelation descriptors,⁶⁸ and eigenvalue-based indices.⁶⁸ All of the descriptors were calculated with Dragon software version 5.4.⁶⁶ The TIs representing all of the compounds described in this study are listed in the Supporting Information.

Linear Discriminant Analysis. LDA is a pattern recognition method that provides a classification model based on the combination of variables that best predict the category or group to which a given compound belongs. Database compounds were allocated to active and inactive groups according to their non-LBP AR antagonist activities. LDA was then applied to these two groups to obtain four discriminant functions, DF₁–DF₄ (eqs 1–4).

The independent variables were the TIs, while the discriminatory property was the non-LBP AR antagonist activity. The discriminant capability was assessed as the percentage of correct classifications in each set of compounds.

The classification criterion was the minimal Mahalanobis distance (the distance of each case to the mean of all of the cases in a category). The quality of the discriminant function was evaluated using the Wilks parameter (λ), which was obtained by multivariate analysis of variance that tests the

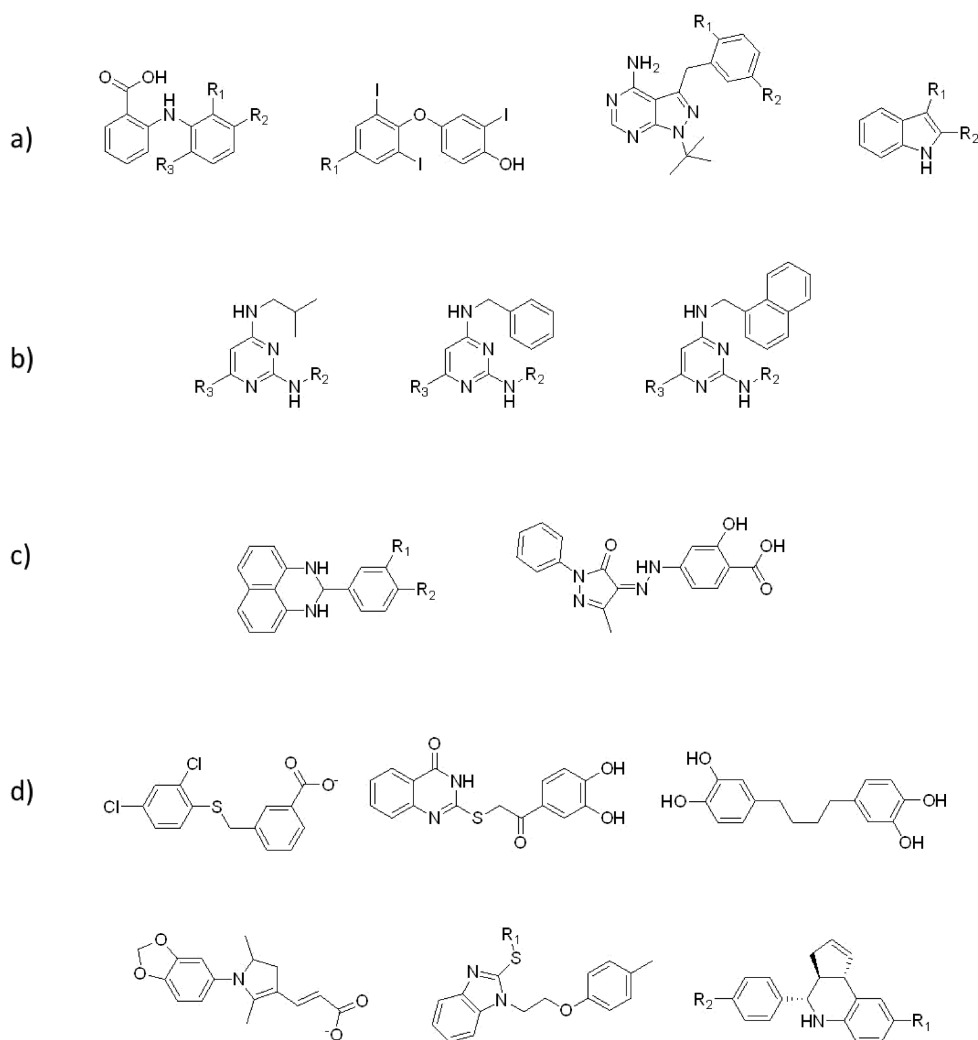


Figure 5. Molecular scaffolds reported in the literature as non-LBP AR antagonists. (a) Estebanez-Perpina et al.² small molecules identified during X-ray screens, including NSAIDS scaffold, TRIAC, and small-molecule fragments. (b) Gunther et al.¹⁰ AR-selective peptidomimetic pyrimidine scaffold identified through structure-based drug design. (c) Axerio-Cilieis et al.¹² AR AF-2-selective scaffolds identified through virtual screening. (d) Lack et al.¹³ AR BF-3-selective scaffolds identified through virtual screening.

equality of group means for the variable in the discriminant model.

The method used to select the descriptors was based on the Fisher–Snedecor parameter (F), which determines the relative importance of candidate variables. The software used for the LDA study was Statistica version 9.0 (StatSoft).⁷⁰

The variables used to compute the linear classification function were chosen in a stepwise manner: at each step, the variable making the largest contribution to the separation of the groups was entered into the discriminant equation (or the variable making the smallest contribution was removed).

Pharmacological Activity Distribution Diagrams. A pharmacological distribution diagram (PDD) is a graphical representation that provides a straightforward way of visualizing the regions of minimum overlap between active and inactive compounds as well as the regions in which the probability of finding active compounds is at maximum.⁷¹ In other words, a PDD is a frequency distribution diagram of dependent variables in which the ordinate axis represents the expectancy of activity (E) and the abscissa represents the DF values in the range. For an arbitrary range of values of a given function, the expectancy of activity is defined as $E = a/(i + 1)$, where a is the number of

active compounds in the range divided by the total number of active compounds and i is the number of inactive compounds in the interval divided by the total number of inactive compounds. The expectancy of inactivity is defined in a symmetrical way as $E' = i/(a + 1)$. Within these diagrams, it is easy to visualize the intervals in which there is a maximum probability of finding new active compounds and a minimum probability of finding inactive compounds.

Molecular Topology Virtual Screening. Two topological virtual screening campaigns were performed. The first one was conducted by applying DF₁ and DF₂ to a group of 17 novel diarylhydrazide analogues synthesized by our group that belong to MDG scaffold 1 [MDG053–MDG069]. After the non-LBP AR antagonist activities of these 17 compounds were experimentally evaluated, the models were refined to obtain two new DFs (DF₃ and DF₄) with increased quality and level of accuracy in predicting novel scaffolds with the desired activity. A second virtual screening based on these two new models (DF₃ and DF₄) was then performed on the SPECS database⁶⁷ to identify novel non-LBP AR antagonist compounds.

General Compound Information. Compounds SPC001–SPC005 were purchased from SPECS.⁶⁷ Compounds

MDG053–MDG069 were synthesized in our laboratories following the experimental procedure previously described.^{72,73} In all instances, the compound purity was greater than 95% as determined by LC–MS and NMR analyses. Compounds were prepared as 10 mM solutions in 100% DMSO.

Time-Resolved Fluorescence Resonance Energy Transfer (TR-FRET). Lanthascreen TR-FRET AR Coactivator Assay Kit (Invitrogen, cat no. PV4381) was used to screen for potential coactivator disruptors. Black low-volume 384-well assay plates (Corning, cat no. 3676) were used to perform the assay (total volume 20 μ L), and the TR-FRET signal was measured with PHERAstar equipment (BMG LabTech) using a Lanthascreen optic module with excitation at 335 nm and emission at 520 nm (channel A) and 495 nm (channel B).

TR-FRET values were calculated at 10 flashes per well using a delay time of 100 μ s and an integration time of 200 μ s, as recommended by the Invitrogen assay guidelines. The intensity ratio (520 nm/495 nm) was then calculated and plotted against the logarithm of the compound concentration. A serial dilution of compounds was first prepared in 100% DMSO (Sigma-Aldrich) starting from the maximum desired concentration to achieve a 12-point concentration range using 96-well polypropylene plates (Nalgene Nunc, Rochester, NY). Each 100 \times solution was diluted to 2 \times concentration with TR-FRET coregulator buffer A (Invitrogen/Life Technologies proprietary buffer), yielding a final concentration of 1% DMSO in each well after all of the additions. Then 10 μ L aliquots of 2 \times compound solutions were added to the 384-well plate in triplicate following the addition of 5 μ L of 4 \times AR LBD (His- and GST-tagged, Invitrogen) and 5 μ L of D11-FxxLF coactivator peptide⁷⁴/terbium (Tb)-labeled anti-GST antibody/dihydrotestosterone (DHT). DHT was included at a concentration equal to its EC₈₀, as determined by running the assay in agonist mode first; the EC₈₀ was calculated as ~7 nM using the following equation:

$$EC_{80} = 10^{[\log EC_{50} + (1/HillSlope) \log[80/(100-80)]]}$$

D11-FxxLF and Tb antibody were premixed in light-protecting vials prior to use. A final DTT concentration of 5 mM was used in the assay buffer in order to prevent protein degradation. All of the plates were incubated for 2–4 h at room temperature protected from light prior to TR-FRET measurement. The data were fit using the sigmoidal dose response (variable slope) function available from GraphPad Prism 5:⁷⁵

$$Y = \text{Bottom} + \frac{\text{Top} - \text{Bottom}}{1 + 10^{[(\log IC_{50} - X) \cdot \text{HillSlope}]}}$$

The Z' factor for these assays was >0.5 as calculated by the equation provided by Zhang et al.⁷⁵

In line with the assay protocol, the known agonist DHT (Sigma, cat no. A8380) and the known antagonist cyproterone acetate (CPA) (Sigma, cat no. C3412), were used as controls in the assay. A background control with no AR LBD present was included to account for diffusion-enhanced FRET or ligand-independent coactivator recruitment. A negative control with 2 \times DMSO was present to account for any solvent vehicle effects. Aggregation/nonspecific mechanisms of inhibition were excluded (see the Supporting Information).

Fluorescence Polarization (FP). PolarScreen Androgen Receptor Competitor Assay Kit Green (Invitrogen, cat no. P3018) was used to investigate the binding of the test compounds to the LBP site, occupied by a high-affinity

fluorophore ligand (Fluormone). First, 100 \times test compound solutions in 100% DMSO were diluted in AR Green buffer (Invitrogen/Life Technologies proprietary buffer) supplemented with 2 mM DTT to achieve 2 \times concentrations, and then 20 μ L of 2 \times compound dilutions were placed in triplicate in a 384-well plate (Corning, cat no. 3576) with 40 μ L volume capacity. Recombinant AR LBD (His- and GST-tagged) and Fluormone AL Green (2 \times) mix were prepared separately in a light-protecting vial, and 20 μ L was then added to each compound dilution to achieve a final LBD and Fluormone concentrations of 50 and 2 nM, respectively, and a final concentration of 1 \times compound. Plates were incubated while protected from light for at least 4 h. Controls included a maximum millipolarization units (mP) positive control consisting of the AR LBD and Fluormone mix (2 \times) and a minimum mP control containing only Fluormone (2 \times). A vehicle control was added to account for the effect of 1% DMSO, and a blank control containing buffer only was also included. The antagonist CPA was included at a final concentration of 50 μ M. Data are presented as percentage of the AR LBD:Fluormone complex. FP was measured with PHERAstar equipment (BMG LabTech) using an optic module with excitation at 485 nm and emission at 530 nm.

PDB Structure Selection. For the theoretical study, X-ray crystal structures of the androgen receptor listed in the sections below were downloaded from the Protein Data Bank (<http://www.pdb.org>) and processed as described below for docking and molecular dynamics (MD) simulations.

Conformer Generation. The generation of conformers for the two enantiomers of compound SPC002 was performed by the LowModeMD method [with a 10 kcal/mol energy gap separation and a root-mean-square deviation (RMSD) of 0.5 for a limit of 1000 conformers] using the MOE 2011.10 package.³

Pharmacophore Generation. Pharmacophores were generated with the Pharmacophore Query implemented in MOE 2011.10. In all cases, ligands were aligned and common features elucidated using the consensus function. To generate the AF-2 pharmacophore, structures 1T7R (androgen receptor) and 3ERD (estrogen receptor) were overlapped, and four common features between the FxxLF and LxxLL motifs, respectively, were selected. To generate a BF-3 pharmacophore, the cocrystallized small molecules in the 2PIU, 2PIO, 2PIV, 2PIX, and 3ZQ7 structures were overlaid, and four common features were selected. The pharmacophores generated were utilized to guide the induced-fit docking, enabling a partial match of at least two features in both cases.

Docking Studies. The structure of human AR LBD (1T63) in complex with the hormone DHT and the coactivator GRIP1 NR box 3 at a resolution of 2.07 Å was prepared using MOE 2011.10. Crystallographic water molecules were removed, and the structure was protonated using the Protonate 3D tool implemented in MOE, leaving the default parameters. The coactivator peptide was subsequently removed, and the amino acids belonging to AF-2 or BF-3 were selected to identify the docking site.

The previously generated (R)-SPC002 and (S)-SPC002 series of conformers were docked using the induced-fit protocol implemented in MOE 2011.10. With this protocol, the site is free to adapt to the ligand during the docking process, and flexibility is allowed for both the ligand and protein side chains within the coactivator binding groove. A pharmacophore restraint was also used to guide the docking of the conformers

into the active site. Docking was limited to 30 maximum poses; the pharmacophore was used as a placement and London dG as a scoring and rescoring function after pose force field refinement. Each induced-fit pose was saved as a separate complex PDB file. The hydrogens were removed from the protein, and then the ligand was individually protonated using the standard MOE protocol.

Molecular Dynamics Simulations. The PDB files of the docked complex structures were converted into an Amber structure file using tLEAP. For the protein, force field parameters and partial charges from the ff99sb force field⁷⁶ were applied. Each ligand pose was prepared using the antechamber module of Amber 11 with the general Amber force field (GAFF)⁷⁷ parameter assignment. Each structure was prepared through a quick optimization step within the Amber force field in vacuum and then placed in a TIP3P water box,⁷⁸ keeping the minimum distance between protein and the walls of the box at 12 Å. Two Cl⁻ counterions were then added to the solvent bulk of protein/water with tLEAP to neutralize the system for MD calculations.

The MD simulations were performed using the Amber 11 software package.⁷⁹ As a starting point for MD simulations, the solvated systems were minimized in a seven-step procedure with variable degrees of freedom. In the first three steps, the steepest-descent method was applied to 1000 steps, followed by 4000 steps of conjugate gradient by restraining the protein backbone using a harmonic potential with a force constant of 50, 5, or 0.5 kcal/mol Å⁻² respectively. In the last four steps, complexes were minimized without any restrictions until the root-mean-square gradient of the potential energy was ≤0.001 kcal/mol.

After minimization, the systems were gradually heated in the NVT ensemble (constant volume and temperature conditions) from 0 to 300 K in 200 ps. Then the systems were equilibrated for 50 ps at a constant temperature of 300 K by coupling the system to a thermal bath using the Berendsen algorithm with a time coupling constant of 1 ps and a pressure of 1 atm (NPT). The SHAKE algorithm was used to constrain the bonds involving hydrogen atoms to their equilibrium values.

MM-PB/GBSA Approach. The molecular mechanics Poisson–Boltzmann/Generalized Born surface area (MM-PB/GBSA) approach⁸⁰ was applied to the last conformation of the seventh minimization step for each of the docked poses to provide the GB and PB *single-point* binding energy values. The five best-ranked poses were brought forward to the MD production step, which consisted of a 10 ns production run in the NVT ensemble maintained at a constant temperature of 300 K by coupling the system to a thermal bath using the Berendsen algorithm with a time coupling constant of 2 ps. Trajectories were analyzed with the ptraj program, and system convergence was evaluated through constant binding free energies (ΔG) during the 10 ns simulation. Binding free energies of the minimized five best docked poses (selected through scoring and single-point MM-PB/GBSA values) were calculated using previously published protocols. Binding free energy calculations were performed using the MM-PB/GBSA method as implemented in Amber 11. On average, 500 snapshots were extracted from the last 5 ns of the trajectory for the calculations. The binding free energy for each calculation is computed from the free energy for each molecular species (complex, protein, and ligand) according to the following equation:

$$\Delta G_{\text{binding}} = G_{\text{complex}} - (G_{\text{protein}} + G_{\text{ligand}})$$

The ΔG values of binding contributions are summarized in the following equation:

$$\Delta G = \Delta G_{\text{MM(gas)}} + \Delta G_{\text{sol}} - T\Delta S$$

where ΔG_{MM} is the molecular mechanics free energy between protein and ligand [sum of the nonbonded electrostatic (Coulombic), van der Waals (Lennard-Jones), and internal energy (bonds, angles and dihedrals in vacuum) contributions], ΔG_{sol} is the solvation free energy, and $T\Delta S$ is the conformational change entropy term. ΔG_{sol} can be expressed as the sum of an electrostatic component ($\Delta G_{\text{ele,sol}}$) and a nonpolar component (ΔG_{np}):

$$\Delta G_{\text{sol}} = \Delta G_{\text{ele,sol}} + \Delta G_{\text{np}}$$

$\Delta G_{\text{ele,sol}}$ values were calculated using internal and external dielectric constants of 1 and 80, corresponding to the dielectric constants of vacuum and water, respectively. The entropy term was omitted because it is very computationally expensive to calculate and it is outside the scope of the present work.

■ RESULTS AND DISCUSSION

Mathematical Modeling. The first equation (eq 1), corresponding to the discriminant function DF₁, distinguished compounds that were predicted as non-LBP AR antagonists using general data available in the literature. In order to obtain DF₁, LDA was applied to a training set composed of 89 compounds distributed into two subsets: active (47 non-LBP AR antagonist compounds described in the literature) and inactive (42 compounds not exhibiting this activity or at least not described as such in the literature) (Table S1 in the Supporting Information). From this first function (eq 1), a given compound is predicted to be active if DF₁ > 0, and otherwise it is classified as inactive. The classification matrix for DF₁ is very significant for the training set: 87% of correct predictions for the active group in DF₁ (i.e., 41 out of 47 compounds) were correctly classified in the active set, whereas 38 out of 42 (90%) were correctly classified in the inactive group.

A second equation (eq 2), corresponding to DF₂, was derived from a group of compounds experimentally assayed for their non-LBP AR antagonist activity by our group. The data set included 52 compounds distributed into two subsets: active (nine non-LBP AR antagonist compounds) and inactive (43 compounds not exhibiting this activity) (Table S2 in the Supporting Information). From this second function (eq 2), a given compound is classified as active (or as a potential non-LBP AR antagonist) if DF₂ > 0, and otherwise it is classified as inactive. The classification matrix for DF₂ is very significant for the training set: 89% of correct predictions for the active group in DF₂ (i.e., eight out of nine compounds) were correctly classified in the active set, whereas 34 out of 43 (79%) were correctly classified in the inactive group.

For these initial models, the equations were composed of two (DF₁) or three (DF₂) independent variables. DF₁ is given by

$$DF_1 = -5.14753 + 2.86118 \cdot EEig09x - 6.42405 \cdot MATS3p \quad (1)$$

where EEig09x is eigenvalue 09 from the edge adjacency matrix weighted by edge degrees and MATS 3p is the Moran autocorrelation-lag 3 weighted by atomic polarizabilities. DF2 is given by

Table 2. Values of DF₁, DF₂, Probability of Activity, and Classification of the New Series of 17 Diarylhydrazide Analogues Synthesized by Our Group

compound	equation 1			equation 2			exp. ^e	IC ₅₀ (μM)
	class. ^a	prob (A) ^b	DF ₁	class.	prob (A)	DF ₂		
AR053	A ^c	0.974	3.641	A	0.753	1.116	I ^d	>100
AR054	A	0.965	3.318	I	0.437	-0.254	A	55
AR055	A	0.962	3.220	A	0.644	0.592	I	>100
AR056	A	0.975	3.657	A	0.990	4.585	I	>100
AR057	A	0.972	3.535	A	0.973	3.572	A	40
AR058	A	0.968	3.415	A	0.967	3.366	A	53
AR059	A	0.908	2.295	A	0.857	1.791	I	>100
AR060	A	0.985	4.211	A	0.634	0.551	A	33
AR061	A	0.976	3.693	A	0.737	1.030	A	13
AR062	A	0.956	3.072	A	0.700	0.849	A	12
AR063	A	0.979	3.821	A	0.978	3.788	I	>100
AR064	A	0.961	3.203	I	0.376	-0.505	I	>100
AR065	A	0.947	2.876	A	0.937	2.703	I	>100
AR066	A	0.923	2.490	A	0.804	1.409	I	>100
AR067	A	0.958	3.122	A	0.992	4.849	I	>100
AR068	A	0.937	2.705	A	0.982	4.009	I	>100
AR069	A	0.911	2.322	A	0.807	1.431	I	>100

^aClassification of the compound. ^bProbability of being an active compound. ^cActive. ^dInactive. ^eExperimental classification of the compound.

$$\begin{aligned} \text{DF}_2 = & -72.44141 + 147.6426 \cdot \text{PW2} + 10.68602 \cdot \text{MATSS5v} \\ & - 10.02955 \cdot \text{GATS4m} \end{aligned} \quad (2)$$

where PW2 is the path/walk 2-Randic shape index, MATSS5v is the Moran autocorrelation-lag 5 weighted by atomic van der Waals volumes, and GATS4m is the Geary autocorrelation-lag 4 weighted by atomic masses. The statistical data and parameters accounting for the significance of these equations were as follows:

$$\text{DF}_1: N = 89, F = 52.77, \lambda = 0.449, p < 0.00001$$

$$\text{DF}_2: N = 52, F = 6.009, \lambda = 0.727, p < 0.0015$$

where *N* is the number of data compounds, λ is the Wilks parameter, *F* is the Fisher–Snedecor parameter, and *p* is the statistical significance.

The mathematical models DF₁ and DF₂ for prediction of non-LBP AR antagonist activity of compounds were then validated on a new series of 17 diarylhydrazide analogues synthesized by our group (Table 1). These compounds were filtered by the two DFs (eqs 1 and 2), and the resulting predicted activities are shown in Table 2. All 17 of the synthesized diarylhydrazide analogues passed the first filter (DF₁) as potential non-LBP AR antagonists. Six of the novel analogues described in Table 1 were described as non-LBP AR antagonists.⁷³ Fifteen of them also passed the second filter (DF₂) as potential non-LBP AR antagonist candidates. As only six candidates were active, our models misclassified 11 of the 17 compounds screened (65%), and hence, further model optimization was needed.

The information retrieved from the experimental data on the diarylhydrazide analogues provided us with greater homogeneous data to build up additional optimized models (DF₃ and DF₄) that were used to carry out a topological virtual screening of the SPECS database (around 200 000 compounds) with the ultimate goal of identifying a novel non-LBP AR antagonist scaffold.

To obtain the discriminant function DF₃, LDA was applied to a training set including 69 compounds distributed into two

subsets: actives (15 non-LBP AR antagonist compounds) and inactives (54 compounds not exhibiting this activity). In this refined model, to the initial nine active MDG compounds included in DF₂ were added the six active compounds from the newly synthesized series of diarylhydrazides (Table S4 in the Supporting Information). From this third function (eq 3), a given compound is selected as active (or as a potential non-LBP AR antagonist) if DF₃ > 0, and otherwise it is classified as inactive. The classification matrix for DF₃ is significant for the training set: 87% of correct predictions for the active group in DF₃ (i.e., 13 out of 15 compounds) were correctly classified in the active set, whereas 37 out of 54 (69%) were correctly classified in the inactive group. This leads to an average correct compound classification percentage of 78%.

Finally, another focused optimized model, DF₄, included six active compounds and 11 inactive compounds from the newly synthesized diarylhydrazide subset of 17 compounds (Table S5 in the Supporting Information). From this fourth model (eq 4), a given compound is selected as active (or as a potential non-LBP AR antagonist) if DF₄ > 0, and otherwise it is classified as inactive. The classification matrix for DF₄ is significant for the training set: 67% of correct predictions for the active group in DF₄ (i.e., four out of six compounds) were correctly classified in the active set, whereas 10 out of 11 (91%) were correctly placed in the inactive group. This leads to an average correct compound classification percentage of 79%.

For these refined models, the equations were composed of two (DF₃) or one (DF₄) independent variable. DF₃ is given by

$$\text{DF}_3 = -4.693 - 3.816 \cdot \text{GATSS5v} + 207.331 \cdot \text{JGI4} \quad (3)$$

where GATSS5v is the Geary autocorrelation-lag 5 weighted by the atomic van der Waals volumes and JGI4 is the mean topological charge index of order 4. DF₄ is given by

$$\text{DF}_4 = -8.979 - 1.705 \cdot \text{SEigp} \quad (4)$$

where SEigp is the eigenvalue sum from the polarizability-weighted distance matrix. The statistical data and parameters accounting for the significance of these equations were as follows:

DF_3 : $N = 69$, $F = 7.15$, $\lambda = 0.822$, $p < 0.0015$

DF_4 : $N = 17$, $F = 8.415$, $\lambda = 0.641$, $p < 0.0110$

The pharmacological distribution diagrams depicted in Figure 6 describe the probabilities of finding active compounds

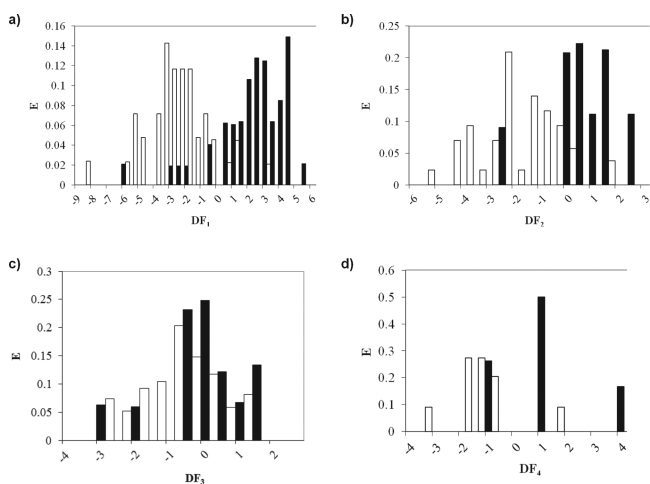


Figure 6. Pharmacological distribution diagrams for non-LBP AR antagonists obtained using the discriminant functions DF_1 – DF_4 . The expectancy of activity (E) is plotted against the DF for each equation. These diagrams establish the DF intervals where the probability of finding active compounds is maximal. The black color represents compounds with predicted non-LBP AR antagonist activity, and the white color represents the inactive compounds.

for the discriminant functions DF_1 – DF_4 applied in our mathematical models to different subsets of compounds. From an analysis of the models' correct classification percentages, we concluded that the DF_3 model is more efficient in identifying active compounds (sensitivity), while the DF_4 model shows better performance in identifying inactive compounds (specificity). This allowed us to advance an interesting strategy to predict non-LBP AR antagonist activity

in a new chemical framework. First, the compounds classified as active by eq 3 (DF_3) were brought forward, and then only those compounds that passed the filter of eq 4 (DF_4) were selected for experimental validation as non-LBP AR antagonists.

Thus, in order to identify new lead compounds with predicted non-LBP AR antagonist activity, the refined models DF_3 and DF_4 were applied to screen the SPECS database of druglike small molecules. The top five scoring compounds from the SPECS database (Figure 7) were selected as candidates for potential non-LBP AR antagonistic activity (Table 3).

Experimental Validation of the Mathematical Models.

SPC002 Disrupts Coactivator Recruitment to the AR LBD with a Non-LBP Mechanism. The five compounds predicted by our molecular topology hypothesis (Figure 7) were purchased from SPECS and evaluated for their ability to disrupt D11-FxxLF coactivator recruitment to DHT-bound AR LBD through TR-FRET at a single-point concentration of 100 μ M. While the other compounds were inactive, **SPC002** was found to inhibit AR coactivator recruitment with an IC_{50} of $\sim 24 \mu$ M (Figure 8a) without displacing a potent fluorescently labeled AR ligand (Fluormone) from the LBP (Figure 8b), differentiating its behavior from the classical LBP antagonist CPA. **SPC002** is a novel compound that can be classified as an AR coactivator binding inhibitor (CBI) with potency comparable to previously described CBIs.

Preliminary Conclusions Based on the Mathematical Models.

Out of the five compounds selected from the virtual screening on the SPECS database, one compound, **SPC002**, demonstrated the predicted biological activity.

No definitive structure–activity relationship conclusions can be drawn solely on the basis of topological models, as only a few compounds are available for comparison. Indeed, considering the indices described in the DF_3 function (GATSSv and JGI4) and the fact that DF_3 is the most important function, we can note that factors related to the molecular polarizability and the intramolecular charge play a role in determining the activity. In this respect, the presence of a triazole group in the molecule **SPC004** causes the JGI4 index value to be excessively large, which places the compound

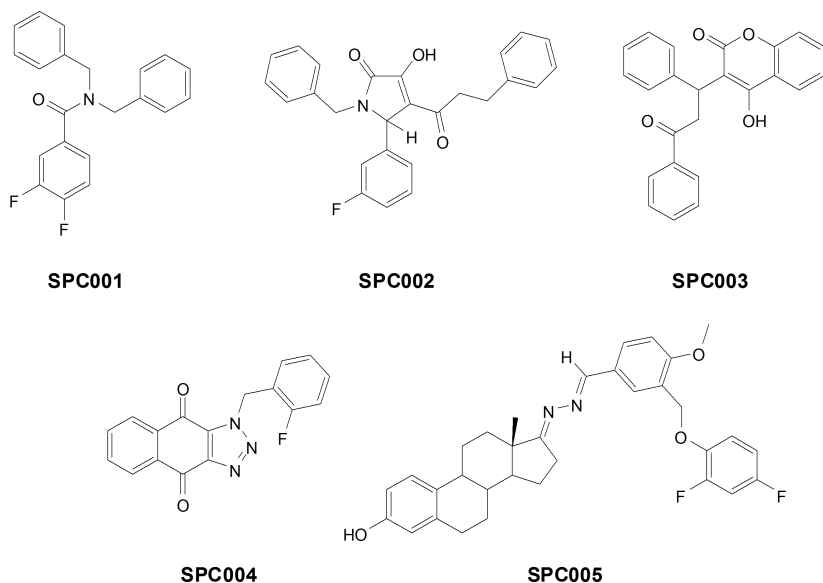


Figure 7. Compounds identified during the second screening campaign on the SPECS database. These compounds were selected after four levels of filtering described by our molecular topology protocol.

Table 3. Values of DF_3 , DF_4 , Probability of Activity, and Classification of the Potential Non-LBP AR Antagonists Screened from the SPECS Database

compound	equation 3		equation 4		exp.	IC_{50} (μM)
	prob (A) ^a	DF_3	prob (A)	DF_4		
SPC001	0.629	0.527	0.802	1.399	I	>100
SPC002	0.612	0.456	0.863	1.838	A	24
SPC003	0.524	0.096	0.946	2.862	I	>100
SPC004	0.906	2.270 (NC ^b)	0.863	1.838	I	>100
SPC005	0.813	1.470	0.946	2.861	I	>100

^aProbability of being an active compound. ^bNC: nonclassified compound (out of the model's range of applicability).

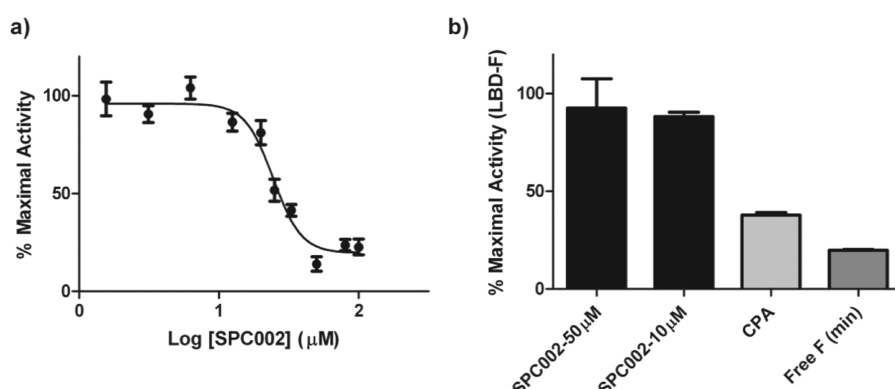


Figure 8. SPC002 disrupts D11-FxxLF coactivator recruitment to the AR LBD with a non-LBP mechanism of action. (a) IC_{50} was measured as $24.4 \pm 2.7 \mu M$ using the slope of the activity vs $\log(\text{antagonist concentration})$ plot. Compounds were tested in a TR-FRET assay across a concentration range from 100 to $1.5 \mu M$ where applicable in the presence of a DHT concentration equal to EC_{80} in wild-type AR LBD. Each data point represents the mean of two independent experiments performed in triplicate. Error bars represent the standard error of the mean (SEM) for $n = 6$ values. The % maximal activity was calculated as previously described.⁸¹ (b) Fluorescence polarization data plotted as the percentage of maximal activity, which is represented by the AR LBD:fluorophore complex (0% inhibition). The minimum control value represents free fluorophore (Free F) in solution (100% inhibition). Error bars represent the SEM for $n = 6$ values.

outside the optimal range of activity. Likewise, the presence of an excess of fluorine atoms produces a low value of the GATSSv index, as demonstrated by compounds **SPC001** and **SPC005**. Conversely, the absence of fluorine atoms in compound **SPC003** makes the GATSSv value too high. Two factors appear to determine the activity of compound **SPC002** related to the optimal range value of the DF_3 function: first, the presence of a single fluorine placed at a topological distance of 5 from the heterocyclic nitrogen, and second, the presence of hydroxyl group at a topological distance of 3 from the carbonyl group.

We can then summarize the results by concluding that compounds **SPC001** and **SPC005** failed to show activity because they present an excessive number of fluorine atoms, **SPC004** failed because of an excess of nitrogens, and **SPC003** failed because of the absence of both F and N. The only active compound, **SPC002**, has one fluorine and one nitrogen placed at an optimal distance from each other. As these results have been interpreted solely on the basis of the indices values of DF_3 , further insight is necessary to derive solid conclusions in terms of structure–activity relationship.

Induced-Fit Docking and Molecular Dynamics Simulations. Given the high interest of the new active compound (**SPC002**), we proceeded to study the possible bioactive conformations of the compound on the AR surface. To do so, a combined protocol of *guided induced-fit docking* and *molecular dynamics simulations* was applied to investigate the possible binding mode of **SPC002** into the two non-LBP binding sites

described on the AR surface, AF-2 and BF-3. Because of the chiral nature of the compound, the protocol was carried out in duplicate, considering independently each of the two enantiomers, (*R*)-**SPC002** and (*S*)-**SPC002**.

Structural information available on the coactivator peptide binding mode at the AR surface guided us to design an AR AF-2 pharmacophore. As shown in Figure 9, three features mimicking the $F_1x_2x_3L_4F_5$ - and $L_1x_2x_3L_4L_5$ -type motifs in the AR AF-2 pocket [one each in subpocket 1 (F_1/L_1 , HydLaro), subpocket 2 (L_4 , HydLaro), and subpocket 3 (F_5/L_5 , HydLaro)] and an additional hydrogen-bond acceptor feature corresponding to the common feature shared by the amino acid x_2 backbone

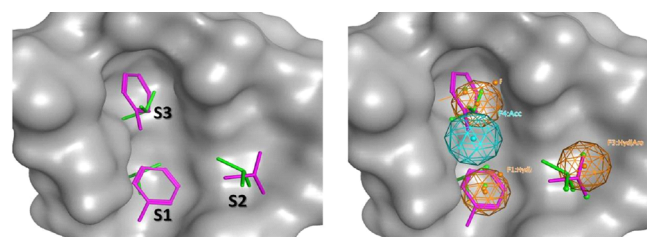


Figure 9. AR AF-2 pharmacophore features. (a) $F_1x_2x_3L_4F_5$ - and $L_1x_2x_3L_4L_5$ -type motifs. The labels S1–S3 denote subpockets 1–3, respectively. (b) Three HydLaro features (orange), corresponding to the F_1/L_1 , L_4 , and F_5/L_5 side chains, and a common acceptor (Acc) feature of the carboxylic group of the x_2 amino acid backbone (light blue). In both panels, the molecular surface is represented in gray. The figure was generated with MOE 2011.10. PDB ID: 1T7R.

were used, enabling the partial match of at least two features, to allow different compound conformations to fit the AF-2 pharmacophore.

To build a BF-3 pharmacophore, we utilized the structural information available from small-molecule cocrystallization previously reported in the literature.² We chose structures 2PIU, 2PIO, 2PIV, 2PIX, and 3ZQ7 to superpose a total of five ligands, from which a common-feature pharmacophore was generated that accounted for four features in total: two hydrophobic, one donor and acceptor, and one general encompassing AroLPiN|Hyd|Don features that represent subpocket S_a1 (Figure 10). A partial match was enabled for two of the four features, allowing different molecule conformations to fit the BF-3 pharmacophore hypothesis.

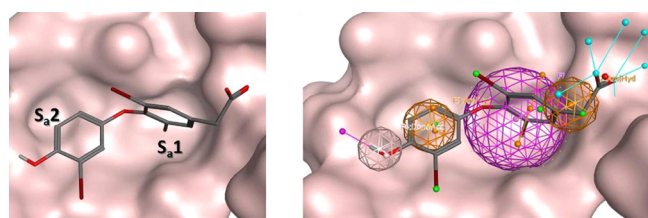


Figure 10. BF-3 pharmacophore for AR. (a) [4-(4-Hydroxy-3-iodophenoxy)-3,5-diiodophenyl]acetic acid (4HY) in the 2PIU structure. The two BF-3 subpockets were arbitrarily called S_a1 and S_a2 to distinguish them from those of AF-2. (b) Two AroLPiN features (orange), one Hyd feature (pink), and a global feature to account for several compound features, such as AroLPiN|Hyd|Don (magenta).

We performed docking of the two enantiomeric series of conformers of **SPC002** previously generated by MOE (78 conformers for the *R* enantiomer and 80 conformers for the *S*

enantiomers) guided by the pharmacophoric features aforementioned both in AF-2 and BF-3. Docking provided the following results: (a) 23 and 22 docked poses on AF-2 for (*R*)- and (*S*)-**SPC002**, respectively, and (b) 25 and 21 docked poses on BF-3 for (*R*)- and (*S*)-**SPC002**, respectively. The four series of poses were ranked as a function of their docking scoring values and refinement energies. All of the AR:**SPC002** complexes were saved as PDB files, minimized using an Amber standard protocol (see the Experimental Section), and reranked on the basis of their binding energies from MM-PB/GBSA single-point calculations on all of the minimized structures (see Supporting Information). Subsequently, the first five or six best-ranked poses considering both the scoring function and MM-PB/GBSA single-point binding energies were selected for further extended analysis, consisting of 10 ns MD simulations. The MM-PB/GBSA average binding energies after the 10 ns MD production run provided the final criterion to identify the most favored pose, which according to our calculations corresponds to pose 15 of the (*S*)-**SPC002** enantiomer in AR AF-2 (Table 4).

Although the energy differences are not very significant, on the basis of our results (Table 4) there would be a predicted higher affinity of compound **SPC002** for the AF-2 site as opposed to the BF-3 site. In addition, this affinity is slightly higher for the *S* enantiomer compared with the *R* enantiomer.

Figure 11 gathers the initial (minimized) and final (after 10 ns) geometries of the best pose identified for each series. The consistency of the conformations during the production step is noteworthy: with the exception of BF-3/(*S*)-**SPC002**, final geometries showed no substantial changes with respect to the initial geometries, and thus validating the efficiency of the docking method employed. This consistency is also reflected for AF-2 complexes in the evolution of ΔG along the MD

Table 4. Pose Selection in AR AF-2 and BF-3^a

site	compound	pose number	E_Score	E_Ref	GB 10 ns	SD	PB 10 ns	SD
AF-2	(<i>R</i>)- SPC002	1	-7.87	-21.59	-21.55	4.00	-17.54	3.67
AF-2	(<i>R</i>)- SPC002	2	-7.11	-22.13	-22.17	3.79	-17.60	3.23
AF-2	(<i>R</i>)- SPC002	5	-6.47	-18.81	-25.76	3.32	-20.23	3.36
AF-2	(<i>R</i>)- SPC002	9	-6.23	-21.39	-17.16	3.66	-15.52	3.39
AF-2	(<i>R</i>)- SPC002	11	-6.12	-21.89	-19.47	3.04	-17.60	3.28
AF-2	(<i>S</i>)- SPC002	4	-7.13	-19.57	-27.04	6.30	-22.11	5.02
AF-2	(<i>S</i>)- SPC002	5	-7.11	-19.31	-29.23	3.90	-23.42	3.25
AF-2	(<i>S</i>)- SPC002	7	-6.81	-20.08	-23.81	3.92	-20.49	3.45
AF-2	(<i>S</i>)- SPC002	8	-6.76	-19.94	-26.45	3.28	-21.03	3.36
AF-2	(<i>S</i>)- SPC002	11	-6.56	-21.44	-21.95	3.97	-18.44	4.20
AF-2	(<i>S</i>)- SPC002	15	-6.47	-18.81	-30.83	3.50	-24.23	3.77
BF-3	(<i>R</i>)- SPC002	1	-8.52	-17.44	-16.14	3.68	-12.52	3.23
BF-3	(<i>R</i>)- SPC002	2	-8.34	-20.13	-17.33	5.49	-13.17	5.68
BF-3	(<i>R</i>)- SPC002	4	-8.04	-17.95	-13.68	4.49	-11.07	3.46
BF-3	(<i>R</i>)- SPC002	6	-7.60	-20.08	-12.76	3.82	-9.78	3.43
BF-3	(<i>R</i>)- SPC002	7	-7.35	-18.15	-18.87	6.16	-13.58	6.28
BF-3	(<i>R</i>)- SPC002	8	-7.29	-23.96	-20.95	3.96	-16.12	4.37
BF-3	(<i>S</i>)- SPC002	1	-10.48	-23.36	-12.80	4.27	-19.31	3.08
BF-3	(<i>S</i>)- SPC002	3	-8.06	-23.02	-12.84	5.24	-18.60	3.25
BF-3	(<i>S</i>)- SPC002	4	-7.75	-17.70	-10.87	3.27	-17.60	2.52
BF-3	(<i>S</i>)- SPC002	10	-6.49	-22.74	-14.34	3.78	-19.01	4.15
BF-3	(<i>S</i>)- SPC002	14	-6.30	-21.27	-12.69	3.31	-17.30	3.36

^aDefinitions: E_score = London dG initial scoring value; E_ref = energy after force field refinement; GB 10 ns and PB 10 ns = mean ΔG values after 10 ns MD simulation using the GB and PB solvation models, respectively; SD = standard deviation. The best pose for each series is set in bold type, and the highest binding energies are indicated with black squares. All energies are reported in kcal/mol.

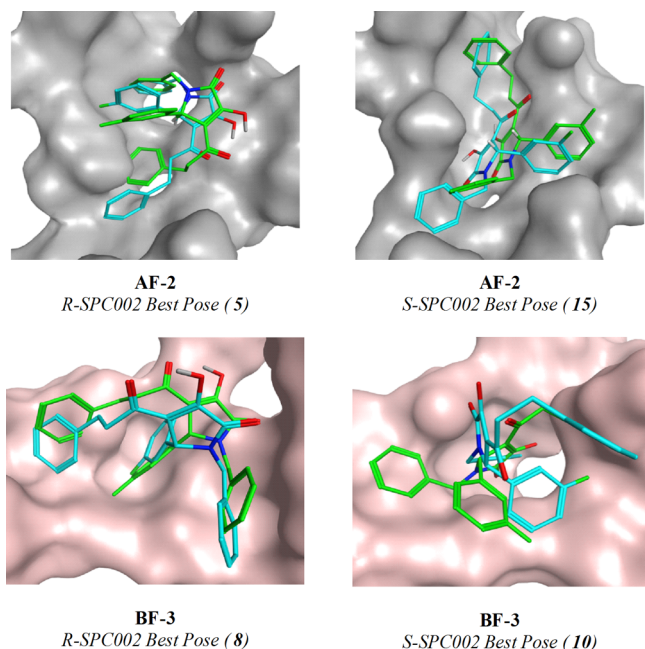


Figure 11. Best poses for (*R*)- and (*S*)-SPC002 in AR AF-2 and AR BF-3. The initial minimized poses are shown in green, while the final optimized poses after 10 ns MD simulations are shown in cyan.

trajectory, which was stable (see Supporting Information). BF-3 complexes, on their part, presented less stable profiles; this was especially significant in the case of the *S* enantiomer, possibly related to the inability of BF-3 to accommodate the compound.

Focusing on the geometry of the complex with the best binding energy, AF-2/(*S*)-SPC002, it is interesting to note the spatial distribution of the compound, which covers the three interacting subpockets previously described for AF-2, placing two phenyl groups in the S1 and S3 regions, mimicking the phenylalanine side chains of the FxxLF motif, and a third fluorophenyl group in the S2 region, which accommodates hydrophobic groups (Figure 12). The accommodation of the phenyl group in the S3 subpocket is further stabilized by π -cation and hydrogen-bonding interactions between lysine residue K720 and the phenyl and carbonyl groups of the ligand moiety, respectively. Furthermore, the pyrrolone linker

presents a carbonyl group placed in close proximity to Q738, which contributes to the stabilization of this pose by a second hydrogen bond. It is interesting to note the relevance of the stereochemistry of the ligand, since this specific highly favorable conformation would not be possible for the *R* enantiomer because of the opposite orientation of the fluorophenyl moiety, which would prevent the stabilizing hydrophobic interaction within the S2 subpocket.

CONCLUSIONS

Molecular topology techniques have been applied to the discovery and preliminary biological characterization of the 1-benzyl-2-(3-fluorophenyl)-4-hydroxy-3-(3-phenylpropanoyl)-2*H*-pyrrole-5-one scaffold as a non-LBP antiandrogen with an IC₅₀ of $\sim 24 \mu\text{M}$ in inhibiting the recruitment of a fluorescently labeled D11-FxxLF coactivator peptide to the AR LBD as determined by TR-FRET.

The mathematical model presented, which is based on the connectivity data of small molecules available in the literature as non-LBP antiandrogens, was able to discriminate between active and inactive compounds successfully and to predict a novel small molecule with the desired biological activity. This scaffold can be further explored for SAR and biological evaluations in terms of its potential applicability in treatment of CRPC.

This report ultimately demonstrates the effectiveness of molecular topology as a drug discovery technique to identify small molecules for challenging targets such as protein–protein interaction interfaces.

ASSOCIATED CONTENT

Supporting Information

Compounds used in the training set and results obtained by applying LDA using eqs 1–4; results of virtual screening on the SPECS database; model building series of compounds; MD simulation protocol, and selected poses for MD simulations. This material is available free of charge via the Internet at <http://pubs.acs.org>.

AUTHOR INFORMATION

Corresponding Authors

*Tel: +1 4154765051. E-mail: laura.caboni@gmail.com (L.C.).
*Tel: +34 963543311. E-mail: maria.galvez@uv.es (M.G.L.).

Present Addresses

[†]L.C.: Department of Biochemistry and Biophysics, University of California, San Francisco, San Francisco, California 94158, United States.

[‡]D.G.L.: Division of Health Sciences, University of South Australia, Adelaide, SA 5000, Australia.

Notes

The authors declare no competing financial interest.

ACKNOWLEDGMENTS

The authors thank the Irish Health Research Board (HRB) (HRB/2007/2), Enterprise Ireland (EI-CFTD/06/110), and the European Commission (Marie-Curie Grant, People FP7, Project Reference 274988) for research funding. The Trinity Biomedical Sciences Institute is supported by a capital infrastructure investment from Cycle 5 of the Irish Higher Education Authority's Programme for Research in Third Level Institutions (PRTLI). Calculations were performed on the Stokes Cluster maintained by the Irish Centre for High-End

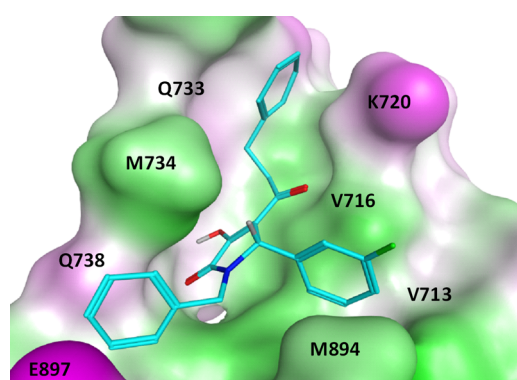


Figure 12. Best pose of compound SPC002 in AR AF-2 as predicted by MD and docking calculations. The AR AF-2 molecular surface is rendered in green and magenta, corresponding to hydrophobic and polar regions, respectively. Images were generated with MOE 2011.10.³

Computing (ICHEC), which is funded by Science Foundation Ireland. The authors thank Dr. Martin Peters for his assistance and the Ministerio de Economía y Competitividad, Spain (Project SAF2009-13059-C03-02) for supporting this study. M.G.-L. acknowledges the “Atracció de Talents” Fellowship provided by the University of Valencia to carry out this study.

■ REFERENCES

- (1) Gronemeyer, H.; Gustafsson, J. A.; Laudet, V. Principles for modulation of the nuclear receptor superfamily. *Nat. Rev. Drug Discovery* **2004**, *3*, 950–964.
- (2) Estebanez-Perpina, E.; Arnold, L. A.; Nguyen, P.; Rodrigues, E. D.; Mar, E.; Bateman, R.; Pallai, P.; Shokat, K. M.; Baxter, J. D.; Guy, R. K.; Webb, P.; Fletterick, R. J. A surface on the androgen receptor that allosterically regulates coactivator binding. *Proc. Natl. Acad. Sci. U.S.A.* **2007**, *104*, 16074–16079.
- (3) Molecular Operating Environment (MOE), version 2011.10; Chemical Computing Group: Montreal, 2011.
- (4) Chang, C. Y.; McDonnell, D. P. Androgen receptor–cofactor interactions as targets for new drug discovery. *Trends Pharmacol. Sci.* **2005**, *26*, 225–228.
- (5) Moore, T. W.; Mayne, C. G.; Katzenellenbogen, J. A. Minireview: Not picking pockets: Nuclear receptor alternate-site modulators (NRAMs). *Mol. Endocrinol.* **2010**, *24*, 683–695.
- (6) Shapiro, D. J.; Mao, C.; Cherian, M. T. Small molecule inhibitors as probes for estrogen and androgen receptor action. *J. Biol. Chem.* **2011**, *286*, 4043–4048.
- (7) Vaz, B.; Mocklinghoff, S.; Brunsved, L. Targeting the Nuclear Receptor–Cofactor Interaction. *Methods Princ. Med. Chem.* **2008**, *39*, 25–45.
- (8) Gao, W. Peptide antagonist of the androgen receptor. *Curr. Pharm. Des.* **2010**, *16*, 1106–1113.
- (9) Estebanez-Perpina, E.; Fletterick, R. J. The Androgen Receptor Coactivator-Binding Interface. In *Androgen Action in Prostate Cancer*; Tindall, D., Mohler, J., Eds.; Springer: New York, 2009; pp 297–314.
- (10) Gunther, J. R.; Parent, A. A.; Katzenellenbogen, J. A. Alternative inhibition of androgen receptor signaling: Peptidomimetic pyrimidines as direct androgen receptor/coactivator disruptors. *ACS Chem. Biol.* **2009**, *4*, 435–440.
- (11) Caboni, L.; Kinsella, G. K.; Blanco, F.; Fayne, D.; Jagoe, W. N.; Carr, M.; Williams, D. C.; Meegan, M. J.; Lloyd, D. G. “True” antiandrogens-selective non-ligand-binding pocket disruptors of androgen receptor–coactivator interactions: Novel tools for prostate cancer. *J. Med. Chem.* **2012**, *55*, 1635–1644.
- (12) Axerio-Cilie, P.; Lack, N. A.; Nayana, M. R.; Chan, K. H.; Yeung, A.; LeBlanc, E.; Guns, E. S.; Rennie, P. S.; Cherkasov, A. Inhibitors of androgen receptor activation function-2 (AF2) site identified through virtual screening. *J. Med. Chem.* **2011**, *54*, 6197–6205.
- (13) Lack, N. A.; Axerio-Cilie, P.; Tavassoli, P.; Han, F. Q.; Chan, K. H.; Feau, C.; LeBlanc, E.; Guns, E. T.; Guy, R. K.; Rennie, P. S.; Cherkasov, A. Targeting the binding function 3 (BF3) site of the human androgen receptor through virtual screening. *J. Med. Chem.* **2011**, *54*, 8563–8573.
- (14) Munuganti, R. S.; LeBlanc, E.; Axerio-Cilie, P.; Labriere, C.; Frewin, K.; Singh, K.; Hassona, M. D.; Lack, N. A.; Li, H.; Ban, F.; Tomlinson Guns, E.; Young, R.; Rennie, P. S.; Cherkasov, A. Targeting the binding function 3 (BF3) site of the androgen receptor through virtual screening. 2. Development of 2-((2-phenoxyethyl)thio)-1*H*-benzimidazole derivatives. *J. Med. Chem.* **2013**, *56*, 1136–1148.
- (15) Caboni, L.; Lloyd, D. G. Beyond the ligand-binding pocket: Targeting alternate sites in nuclear receptors. *Med. Res. Rev.* **2013**, *33*, 1081–1118.
- (16) Sun, A.; Moore, T. W.; Gunther, J. R.; Kim, M. S.; Rhoden, E.; Du, Y.; Fu, H.; Snyder, J. P.; Katzenellenbogen, J. A. Discovering small-molecule estrogen receptor α /coactivator binding inhibitors: High-throughput screening, ligand development, and models for enhanced potency. *ChemMedChem* **2011**, *6*, 654–666.
- (17) Garcia-Domenech, R.; de Julian-Ortiz, J. V.; Duart, M. J.; Garcia-Torrecillas, J. M.; Anton-Fos, G. M.; Rios-Santamarina, I.; de Gregorio-Alapont, C.; Galvez, J. Search of a topological pattern to evaluate toxicity of heterogeneous compounds. *SAR QSAR Environ. Res.* **2001**, *12*, 237–254.
- (18) Garcia-Domenech, R.; Alarcon-Elbal, P.; Bolas, G.; Bueno-Mari, R.; Chorda-Olmos, F. A.; Delacour, S. A.; Mourino, M. C.; Vidal, A.; Galvez, J. Prediction of acute toxicity of organophosphorus pesticides using topological indices. *SAR QSAR Environ. Res.* **2007**, *18*, 745–755.
- (19) Garcia-Domenech, R.; Villanueva, A.; Galvez, J. Application of molecular topology for the prediction of the toxicity of organic chemicals to *Chlorella vulgaris*. *Org. Chem.: Indian J.* **2008**, *4*, 470–474.
- (20) Duart, M. J.; Anton-Fos, G. M.; de Julian-Ortiz, J. V.; Gozalbes, R.; Galvez, J.; Garcia-Domenech, R. Use of molecular topology for the prediction of physico-chemical, pharmacokinetic and toxicological properties of a group of antihistaminic drugs. *Int. J. Pharm.* **2002**, *246*, 111–119.
- (21) Galvez, J.; Galvez-Lloparr, M.; Garcia-Domenech, R. Molecular topology as a novel approach for drug discovery. *Expert Opin. Drug Discovery* **2012**, *7*, 133–153.
- (22) Garcia-Domenech, R.; Galvez, J.; de Julian-Ortiz, J. V.; Pogliani, L. Some new trends in chemical graph theory. *Chem. Rev.* **2008**, *108*, 1127–1169.
- (23) Galvez, J.; Garcia-Domenech, R.; de Julian-Ortiz, J. V.; Soler, R. Topological approach to drug design. *J. Chem. Inf. Comput. Sci.* **1995**, *35*, 272–284.
- (24) Galvez, J.; Galvez-Lloparr, M.; Garcia-Domenech, R. Introduction to molecular topology: Basic concepts and application to drug design. *Curr. Comput.-Aided Drug Des.* **2012**, *8*, 196–223.
- (25) Galvez, J.; Villar, V. M.; Galvez-Lloparr, M.; Amigo, J. M. Chemistry explained by topology: An alternative approach. *Comb. Chem. High Throughput Screening* **2011**, *14*, 279–283.
- (26) Galvez, J. On a topological interpretation of electronic and vibrational molecular energies. *Comput. Theor. Chem.* **1998**, *429*, 255–264.
- (27) de Julian-Ortiz, J. V.; de Gregorio Alapont, C.; Rios-Santamarina, I.; Garcia-Domenech, R.; Galvez, J. Prediction of properties of chiral compounds by molecular topology. *J. Mol. Graphics Modell.* **1998**, *16*, 14–18.
- (28) Castillo-Garit, J. A.; Marrero-Ponce, Y.; Torrens, F.; Garcia-Domenech, R.; Romero-Zaldivar, V. Bond-based 3D-chiral linear indices: Theory and QSAR applications to central chirality codification. *J. Comput. Chem.* **2008**, *29*, 2500–2512.
- (29) Galvez, J. A graph-theoretical approach to calculate vibrational energies of atomic and subatomic systems. *Open J. Phys. Chem.* **2012**, *2*, 204–211.
- (30) Gálvez, J.; Parreño, M.; Pla, J.; Sanchez, J.; Gálvez-Lloparr, M.; Navarro, S.; García-Domenech, R. Application of Molecular Topology to the Prediction of Water Quality Indices of Alkylphenol Pollutants. *Int. J. Chemoinf. Chem. Eng.* **2011**, *1*, 1–11.
- (31) García-Domenech, R.; Catalá, A. I.; García-García, A.; Soriano, A.; Pérez-Mondéjar, V.; Gálvez, J. QSAR by molecular topology of 2,4-dihydroxythiobenzanilides—A virtual screening approach to optimize the antifungal activity. *Indian J. Chem., Sect. B* **2002**, *41B*, 2376–2384.
- (32) Galvez-Lloparr, M.; Giner, R. M.; Recio, M. C.; Candeletti, S.; Garcia-Domenech, R. Application of Molecular Topology to the Search of Novel NSAIDs: Experimental Validation of Activity. *Lett. Drug Des. Discovery* **2010**, *7*, 438–445.
- (33) de Julian-Ortiz, J. V.; Galvez, J.; Munoz-Collado, C.; Garcia-Domenech, R.; Gimeno-Cardona, C. Virtual combinatorial syntheses and computational screening of new potential anti-herpes compounds. *J. Med. Chem.* **1999**, *42*, 3308–3314.
- (34) Bruno-Blanch, L.; Galvez, J.; Garcia-Domenech, R. Topological virtual screening: A way to find new anticonvulsant drugs from chemical diversity. *Bioorg. Med. Chem. Lett.* **2003**, *13*, 2749–2754.
- (35) Rios-Santamarina, I.; Garcia-Domenech, R.; Galvez, J.; Cortijo, J.; Santamaria, P.; Morcillo, E. New bronchodilators selected by molecular topology. *Bioorg. Med. Chem. Lett.* **1998**, *8*, 477–482.

- (36) Duart, M. J.; Garcia-Domenech, R.; Anton-Fos, G. M.; Galvez, J. Optimization of a mathematical topological pattern for the prediction of antihistaminic activity. *J. Comput.-Aided Mol. Des.* **2001**, *15*, 561–572.
- (37) Galvez, J.; Garcia-Domenech, R.; Gomez-Lechon, M. J.; Castell, J. V. Use of molecular topology in the selection of new cytostatic drugs. *Comput. Theor. Chem.* **2000**, *504*, 241–248.
- (38) de Gregorio Alapont, C.; Garcia-Domenech, R.; Galvez, J.; Ros, M. J.; Wolski, S.; Garcia, M. D. Molecular topology: A useful tool for the search of new antibacterials. *Bioorg. Med. Chem. Lett.* **2000**, *10*, 2033–2036.
- (39) Duart, M. J.; Anton-Fos, G. M.; Aleman, P. A.; Gay-Roig, J. B.; Gonzalez-Rosende, M. E.; Galvez, J.; Garcia-Domenech, R. New potential antihistaminic compounds. Virtual combinatorial chemistry, computational screening, real synthesis, and pharmacological evaluation. *J. Med. Chem.* **2005**, *48*, 1260–1264.
- (40) Gozalbes, R.; Brun-Pascaud, M.; Garcia-Domenech, R.; Galvez, J.; Girard, P. M.; Doucet, J. P.; Derouin, F. Anti-toxoplasma activities of 24 quinolones and fluoroquinolones in vitro: Prediction of activity by molecular topology and virtual computational techniques. *Antimicrob. Agents Chemother.* **2000**, *44*, 2771–2776.
- (41) Garcia-March, F. J.; Garcia-Domenech, R.; Galvez, J.; Anton-Fos, G. M.; de Julian-Ortiz, J. V.; Giner-Pons, R.; Recio-Iglesias, M. C. Pharmacological studies of 1-(*p*-chlorophenyl)propanol and 2-(1-hydroxy-3-but enyl)phenol: Two new non-narcotic analgesics designed by molecular connectivity. *J. Pharm. Pharmacol.* **1997**, *49*, 10–15.
- (42) Garcia-Domenech, R.; Domingo-Puig, C.; Esteve-Martinez, M. A.; Schmitt, J.; Vera-Martinez, J.; Chindemi, A. L.; Galvez, J. Aplicacion de la topologia molecular en la busqueda de nuevos agentes activos frente a leishmania. *An. R. Acad. Nac. Farm.* **2008**, *74*, 345–367.
- (43) Garcia-Domenech, R.; Lopez-Pena, W.; Sanchez-Perdomo, Y.; Sanders, J. R.; Sierra-Araujo, M. M.; Zapata, C.; Galvez, J. Application of molecular topology to the prediction of the antimalarial activity of a group of uracil-based acyclic and deoxyuridine compounds. *Int. J. Pharm.* **2008**, *363*, 78–84.
- (44) Garcia-Domenech, R.; Aguilera, J.; Moncef, A. E.; Pocovi, S.; Galvez, J. Application of molecular topology to the prediction of mosquito repellents of a group of terpenoid compounds. *Mol. Diversity* **2010**, *14*, 321–329.
- (45) Gozalbes, R.; Brun-Pascaud, M.; Garcia-Domenech, R.; Galvez, J.; Girard, P. M.; Doucet, J. P.; Derouin, F. Prediction of quinolone activity against *Mycobacterium avium* by molecular topology and virtual computational screening. *Antimicrob. Agents Chemother.* **2000**, *44*, 2764–2770.
- (46) Pastor, L.; Garcia-Domenech, R.; Galvez, J.; Wolski, S.; Garcia, M. D. New antifungals selected by molecular topology. *Bioorg. Med. Chem. Lett.* **1998**, *8*, 2577–2582.
- (47) Gozalbes, R.; Galvez, J.; Garcia-Domenech, R.; Derouin, F. Molecular search of new active drugs against *Toxoplasma gondii*. SAR QSAR Environ. Res. **1999**, *10*, 47–60.
- (48) Galvez, J.; Garcia-Domenech, R.; de Julian-Ortiz, V.; Soler, R. Topological approach to analgesia. *J. Chem. Inf. Comput. Sci.* **1994**, *34*, 1198–1203.
- (49) Galvez-Llompert, M.; Recio, M. C.; Garcia-Domenech, R. Topological virtual screening: A way to find new compounds active in ulcerative colitis by inhibiting NF- κ B. *Mol. Diversity* **2011**, *15*, 917–926.
- (50) Estrada, E.; Pena, A.; Garcia-Domenech, R. Designing sedative/hypnotic compounds from a novel substructural graph-theoretical approach. *J. Comput.-Aided Mol. Des.* **1998**, *12*, 583–595.
- (51) Pla-Franco, J.; Galvez-Llompert, M.; Galvez, J.; Garcia-Domenech, R. Application of molecular topology for the prediction of reaction yields and anti-inflammatory activity of heterocyclic amidine derivatives. *Int. J. Mol. Sci.* **2011**, *12*, 1281–1292.
- (52) Marrero-Ponce, Y.; Siverio-Mota, D.; Galvez-Llompert, M.; Recio, M. C.; Giner, R. M.; Garcia-Domenech, R.; Torrens, F.; Aran, V. J.; Cordero-Maldonado, M. L.; Esguera, C. V.; de Witte, P. A.; Crawford, A. D. Discovery of novel anti-inflammatory drug-like compounds by aligning in silico and in vivo screening: The nitroindazolinone chemotype. *Eur. J. Med. Chem.* **2011**, *46*, 5736–5753.
- (53) Casaban-Ros, E.; Anton-Fos, G. M.; Galvez, J.; Duart, M. J.; Garcia-Domenech, R. Search for new antihistaminic compounds by molecular connectivity. *Quant. Struct.-Act. Relat.* **1999**, *18*, 35–42.
- (54) Galvez-Llompert, M.; Zanni, R.; Garcia-Domenech, R. Modeling natural anti-inflammatory compounds by molecular topology. *Int. J. Mol. Sci.* **2011**, *12*, 9481–9503.
- (55) Mahmoudi, N.; de Julian-Ortiz, J. V.; Ciceron, L.; Galvez, J.; Mazier, D.; Danis, M.; Derouin, F.; Garcia-Domenech, R. Identification of new antimalarial drugs by linear discriminant analysis and topological virtual screening. *J. Antimicrob. Chemother.* **2006**, *57*, 489–497.
- (56) Anton-Fos, G. M.; Garcia-Domenech, R.; Perez-Gimenez, F.; Peris-Ribera, J. E.; Garcia-March, F. J.; Salabert-Salvador, M. T. Pharmacological studies of the two new hypoglycaemic compounds 4-(3-methyl-5-oxo-2-pyrazolin-1-yl)benzoic acid and 1-(mesitylen-2-sulfonyl)-1H-1,2,4-triazole. *Arzneim. Forsch.* **1994**, *44*, 821–826.
- (57) Galvez, J.; Gomez-Lechon, M.; Garcia-Domenech, R.; Castell, J. V. New cytostatic agents obtained by molecular topology. *Bioorg. Med. Chem. Lett.* **1996**, *6*, 2301–2306.
- (58) Garcia-Domenech, R.; Garcia-March, F.; Soler, R.; Galvez, J.; Anton-Fos, G. M.; de Julian-Ortiz, J. V. New analgesics designed by molecular topology. *QSAR* **1996**, *15*, 201–207.
- (59) Galvez-Llompert, M.; Galvez, J.; Garcia-Domenech, R.; Kier, L. B. Modeling drug-induced anorexia by molecular topology. *J. Chem. Inf. Model.* **2012**, *S2*, 1337–1344.
- (60) Galvez-Llompert, M.; Galvez, J.; Garcia-Domenech, R.; Kier, L. B. Predicting Dyspnea Inducers by Molecular Topology. *J. Chem.* **2013**, No. 798508.
- (61) Jasinski, P.; Welsh, B.; Galvez, J.; Land, D.; Zwolak, P.; Ghandi, L.; Terai, K.; Dudek, A. Z. A novel quinoline, MT477: Suppresses cell signaling through Ras molecular pathway, inhibits PKC activity, and demonstrates *in vivo* anti-tumor activity against human carcinoma cell lines. *Invest. New Drugs* **2008**, *26*, 223–232.
- (62) Mahmoudi, N.; Garcia-Domenech, R.; Galvez, J.; Farhati, K.; Franetich, J. F.; Sauerwein, R.; Hannoun, L.; Derouin, F.; Danis, M.; Mazier, D. New active drugs against liver stages of *Plasmodium* predicted by molecular topology. *Antimicrob. Agents Chemother.* **2008**, *S2*, 1215–1220.
- (63) Galvez, J.; Garcia-Domenech, R.; Garcia-March, F.; Moliner-Llusar, R. Derivados del 1-(2,4 dimetil)fenil etanona. Compuestos con aplicaciones farmacológicas por su actividad analgésica y antiinflamatoria. 1991
- (64) Galvez, J.; Garcia-Domenech, R.; Garcia-March, F.; Moliner-Llusar, R. Derivados del 2-(1-propenil) fenol. Compuestos con aplicaciones farmacológicas por su actividad analgésica y antiinflamatoria. 1991
- (65) Galvez, J.; Llompert, J.; Land, D.; Pasinetti, G. Compositions for treatment of Alzheimer's disease. WO2010114636 A1, 2010.
- (66) Dragon, version 5.4; Talete srl: Milano, Italy, 2006.
- (67) SPECS Database; SPECS NV: Delft, The Netherlands.
- (68) Todeschini, R.; Consonni, V. *Molecular Descriptors for Chemoinformatics: Methods and Principles in Medicinal Chemistry*, Vol. 41; Wiley-VCH: Weinheim, Germany, 2009.
- (69) Galvez, J.; Garcia, R.; Salabert, M. T.; Soler, R. Charge Indexes—New Topological Descriptors. *J. Chem. Inf. Comput. Sci.* **1994**, *34*, 520–525.
- (70) Statistica, version 9.0; Statsoft: Tulsa, OK, 2009.
- (71) Galvez, J.; Garcia-Domenech, R.; de Gregorio Alapont, C.; de Julian-Ortiz, J. V.; Popa, L. Pharmacological distribution diagrams: A tool for de novo drug design. *J. Mol. Graphics* **1996**, *14*, 272–276.
- (72) Blanco, F.; Egan, B.; Caboni, L.; Elguero, J.; O'Brien, J.; McCabe, T.; Payne, D.; Meegan, M. J.; Lloyd, D. G. Study of *E/Z* isomerization in a series of novel non-ligand binding pocket androgen receptor antagonists. *J. Chem. Inf. Model.* **2012**, *S2*, 2387–2397.
- (73) Caboni, L.; Egan, B.; Kelly, B.; Blanco, F.; Payne, D.; Meegan, M. J.; Lloyd, D. G. Structure–activity relationships in non-ligand

- binding pocket (non-LBP) diarylhydrazide antiandrogens. *J. Chem. Inf. Model.* **2013**, *53*, 2116–2130.
- (74) He, B.; Minges, J. T.; Lee, L. W.; Wilson, E. M. The FXXLF motif mediates androgen receptor-specific interactions with coregulators. *J. Biol. Chem.* **2002**, *277*, 10226–10235.
- (75) Zhang, J. H.; Chung, T. D.; Oldenburg, K. R. A Simple Statistical Parameter for Use in Evaluation and Validation of High Throughput Screening Assays. *J. Biomol. Screening* **1999**, *4*, 67–73.
- (76) Hornak, V.; Abel, R.; Okur, A.; Strockbine, B.; Roitberg, A.; Simmerling, C. Comparison of multiple Amber force fields and development of improved protein backbone parameters. *Proteins* **2006**, *65*, 712–725.
- (77) Wang, J.; Wolf, R. M.; Caldwell, J. W.; Kollman, P. A.; Case, D. A. Development and testing of a general Amber force field. *J. Comput. Chem.* **2004**, *25*, 1157–1174.
- (78) Jorgensen, W. L.; Chandrasekhar, J.; Madura, J. D.; Impey, R. W.; Klein, M. L. Comparison of Simple Potential Functions for Simulating Liquid Water. *J. Chem. Phys.* **1983**, *79*, 926–935.
- (79) Case, D. A.; Darden, T. A.; Cheatham, T. E., III; Simmerling, C. L.; Wang, J.; Duke, R. E.; Luo, R.; Walker, R. C.; Zhang, W.; Merz, K. M.; Roberts, B.; Wang, B.; Hayik, S.; Roitberg, A.; Seabra, G.; Kolossváry, I.; Wong, K. F.; Paesani, F.; Vanicek, J.; Liu, J.; Wu, X.; Brozell, S. R.; Steinbrecher, T.; Gohlke, H.; Cai, Q.; Ye, X.; Wang, J.; Hsieh, M. J.; Cui, G.; Roe, D. R.; Mathews, D. H.; Seetin, M. G.; Sagui, C.; Babin, V.; Luchko, T.; Gusarov, S.; Kovalenko, A.; Kollman, P. A. *AMBER 11*; University of California: San Francisco, 2010.
- (80) Kollman, P. A.; Massova, I.; Reyes, C.; Kuhn, B.; Huo, S.; Chong, L.; Lee, M.; Lee, T.; Duan, Y.; Wang, W.; Donini, O.; Cieplak, P.; Srinivasan, J.; Case, D. A.; Cheatham, T. E., III. Calculating structures and free energies of complex molecules: Combining molecular mechanics and continuum models. *Acc. Chem. Res.* **2000**, *33*, 889–897.
- (81) Gunther, J. R.; Du, Y.; Rhoden, E.; Lewis, I.; Revennaugh, B.; Moore, T. W.; Kim, S. H.; Dingledine, R.; Fu, H.; Katzenellenbogen, J. A. A set of time-resolved fluorescence resonance energy transfer assays for the discovery of inhibitors of estrogen receptor-coactivator binding. *J. Biomol. Screening* **2009**, *14*, 181–193.